Electron-impact single ionization of low-charged molybdenum ions

D. Hathiramani, K. Aichele, G. Hofmann, M. Steidl, M. Stenke, R. Völpel, and E. Salzborn
Institut für Kernphysik, University of Giessen, D-35392 Giessen, Germany

M. S. Pindzola and J. A. Shaw
Department of Physics, Auburn University, Auburn, Alabama 36849

D. C. Griffin
Department of Physics, Rollins College, Winter Park, Florida 32789

N. R. Badnell
Department of Physics and Applied Physics, University of Strathclyde, Glasgow G4 0NG, United Kingdom
(Received 27 December 1995)

The electron-impact single ionization of low-charged Mo ions is studied both experimentally and theoretically. The absolute cross sections for Mo^{q+} ions in charge states $q=1-8$ are measured using a crossed-beam technique. Distorted-wave calculations are made including both direct ionization and excitation-autoionization contributions. For ions in charge states $q=6-8$, the measured cross sections are in good agreement with calculations involving only the lowest-energy metastable configuration. For ions in charge states $q=3-8$, the good agreement between experiment and theory confirms the dominant role played by excitation-autoionization contributions to the total ionization cross section. [S1050-2947(96)07807-9]

PACS number(s): 34.80.Kw, 34.80.Dp

I. INTRODUCTION

A better understanding of atomic collision processes involving low-charged ions is important for the modeling of fusion edge plasmas [1]. The use of a molybdenum surface for divertor plates in tokamaks is currently under experimental investigation in Alcator C-Mod at the Massachusetts Institute of Technology and in FTU at the Centro Richerche Energia in Frascati. These experiments will pave the way for future use of metal divertors on the next generation of fusion machines.

The atomic collision data for electron-impact single ionization of low-charged Mo ions are sparse. In the past, electron ionization cross sections have been measured for Mo^{+} [2] and calculated for Mo^{11+}, Mo^{12+}, Mo^{13+} [3,4], and Mo^{31+} [5]. Ionization rate coefficients have also been calculated for Mo^{8+}, Mo^{9+}, and Mo^{10+} [4], although only for the ground configurations. In this paper we report on a joint experimental and theoretical project that extends the recent study of Bannister *et al.* [6] on Mo^{4+} and Mo^{5+} to cover the electron-impact single ionization of all Mo^{q+} ions from $q=1$ to 8. Strong excitation-autoionization contributions to the total ionization cross section are confirmed for Mo^{q+} ions from $q=3$ to 8. We also find for Mo^{q+} ions from $q=6$ to 8 that ionization from the lowest-energy metastable configuration dominates the measured cross sections.

The remainder of the paper is partitioned as follows: in Sec. II we outline the crossed-beam experimental method, in Sec. III we review distorted-wave theory as applied to the electron-impact ionization of atomic ions, in Sec. IV we compare experiment and theory for Mo^{+} through Mo^{8+}, while in Sec. V we give a brief summary.

II. CROSSED-BEAM EXPERIMENTAL METHOD

The measurements were performed at the Giessen electron-ion crossed-beam setup (Fig. 1), which has been described in detail earlier [7,8]. The molybdenum ions were produced by a 10-GHz electron cyclotron resonance (ECR) ion source [9] using the insertion technique (Fig. 2), where a bundle of thin 0.5-mm-diam molybdenum wires mounted on top of a rod was fed axially to the edge of the ECR plasma. With this technique the ion source was in operation for nearly 10 h before the bundle of molybdenum wires had to be replaced.

Ion currents of some nA of Mo^{+} up to Mo^{8+} ions at 10-kV acceleration voltage have been obtained. The low ion current was caused by the unfavorable isotope distribution of molybdenum, where ^{98}Mo is the stable isotope with the largest partition (24.1%) in the natural mixture. Molybdenum ions of mass 98 amu were used for the present investigation. Only the cross section of the single ionization of Mo^{7+} was measured with the isotope ^{92}Mo, because $^{98}Mo^{7+}$ ions have the same mass-to-charge ratio as $^{14}N^{+}$.

After analysis for the desired mass-to-charge ratio and a tight collimation to typically 1-mm diameter, which reduced the beam current roughly by a factor of 100, the ion beam was crossed with an intense electron beam. We employed two different types of electron guns. A high-current electron gun delivers a ribbon-shaped electron beam at energies from 10 to 1000 eV and currents up to 450 mA [10]. The second type is a newly developed high-energy electron gun with an axial symmetric setup. This gun is designed for the electron energy range from 50 to 6500 eV and delivers electron currents up to 430 mA [11]. After the electron-ion interaction, the product ions were separated from the incident ion beam by a magnetic field and detected by a single particle detector.

 © 1996 The American Physical Society

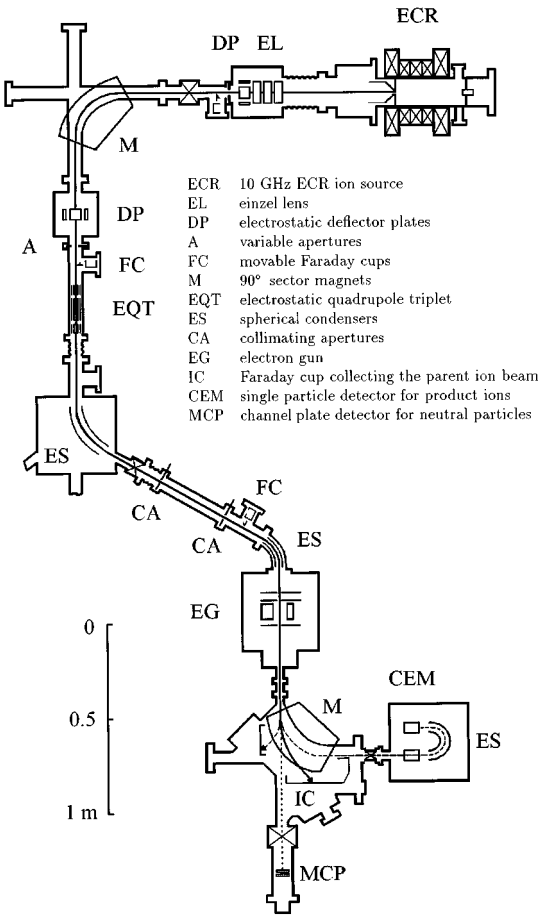

FIG. 1. Schematic view of the experimental setup, including the whole beamline from the ion source to the detector.

The incident ion beam was collected in a large Faraday cup. Absolute cross sections were obtained by employing the dynamic crossed-beam technique [12], where the electron gun is moved up and down through the ion beam with simultaneous registration of the ion signal and both actual beam currents. The total experimental uncertainties of the measured cross sections are typically 8% at the maximum resulting from the quadrature sum of the nonstatistical errors of about 7.8% and the statistical error at 90% confidence level.

III. DISTORTED-WAVE THEORETICAL METHOD

Major contributions to the electron-impact single-ionization cross section are made by the following two processes:

$$e^- + A^{q+} \rightarrow A^{(q+1)+} + e^- + e^-, \tag{1}$$

and

$$e^- + A^{q+} \rightarrow (A^{q+})^* + e^- \rightarrow A^{(q+1)+} + e^- + e^-, \tag{2}$$

where A represents an arbitrary ion with charge q. The first process is direct ionization while the second is excitation autoionization. Since for low-charged ions the branching ratio for autoionization is approximately one, the total ionization cross section is given by

$$\sigma_{\rm tot} = \sum_f \sigma_{\rm ion}(i \rightarrow f) + \sum_j \sigma_{\rm exc}(i \rightarrow j), \tag{3}$$

where $\sigma_{\rm ion}(i \rightarrow f)$ is the direct ionization cross section from an initial configuration, term, or level i of the N-electron ion to a final configuration, term, or level f of the $(N-1)$-electron ion and $\sigma_{\rm exc}(i \rightarrow j)$ is the inner-shell excitation cross section from an initial configuration, term, or level i of the N-electron ion to an autoionizing configuration, term, or level j of the N-electron ion.

The direct ionization and inner-shell excitation cross sections for all the Mo^{q+} ions are calculated in a configuration-average distorted-wave approximation [13]. The threshold energies and bound radial orbitals needed to evaluate the cross sections are calculated using the relativistically corrected Hartree-Fock atomic structure code of Cowan [14,15]. A prior form of the scattering amplitude and a maximum interference approximation [16] are employed to evaluate the

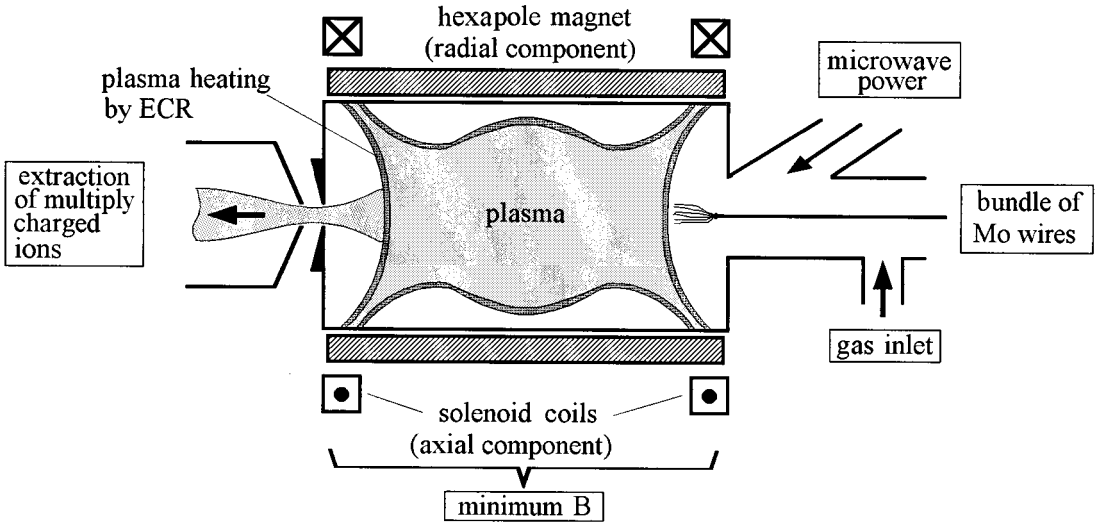

FIG. 2. Principle of the ECR ion source with the bundle of molybdenum wires.

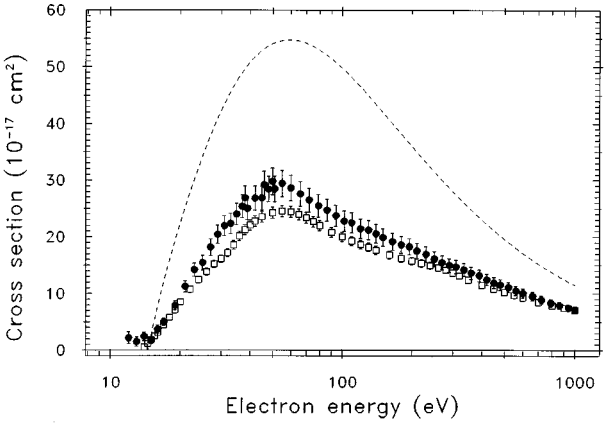

FIG. 3. Electron-impact single ionization of Mo^+. Solid circles: present measurements; open squares: measurements of Man, Smith, and Harrison [2]; dashed curve: direct ionization from the $4p^6 4d^5$ ground configuration.

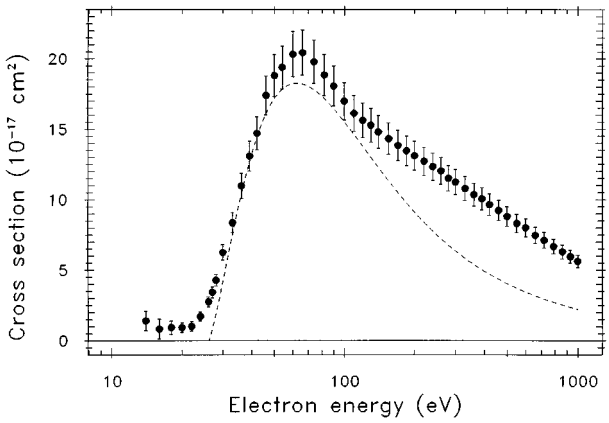

FIG. 4. Electron-impact single ionization of Mo^{2+}. Solid circles: present measurements; dashed curve: direct ionization from the $4p^6 4d^4$ ground configuration.

direct ionization cross sections.

More accurate inner-shell excitation cross sections for Mo^{3+} are calculated in a multiconfiguration *LSJ* level resolved distorted-wave approximation. Threshold energies, bound radial orbitals, and term and level mixing coefficients are calculated using the atomic structure package of Fischer [17]. Nonrelativistic *LS* scattering algebra is generated using a modified version of the general angular momentum code of Scott and Hibbert [18]. Following standard methods [19], the nonrelativistic *K* matrices are then transformed from *LS* to *jK* coupling, followed by a further transformation to intermediate coupling through the use of ''term coupling'' coefficients. The resulting relativistic *K* matrices yield level-to-level cross sections and rate coefficients.

IV. COMPARISON BETWEEN EXPERIMENT AND THEORY

The electron-impact single ionization cross sections for Mo^{q+} ions in charge states $q=1$ to 8 are shown in Figs. 3–11. The error bars indicate a total experimental uncertainty.

A. Mo^+ and Mo^{2+}

Two crossed-beam experimental measurements for the ionization cross section of Mo^+ are compared with distorted-wave theory in Fig. 3. At 50-eV incident energy, near the peak of the cross section, the present measurements are about 25% higher than the previous measurements of Man, Smith, and Anderson [2]. The configuration-average distorted-wave calculation for $4d$ subshell direct ionization from the $4p^6 4d^5$ ground configuration is almost a factor of 2 higher than the present measurements. Direct ionization of the $4p$ subshell will contribute to the double ionization of Mo^+. A configuration-average calculation for the $4p \rightarrow 4d$ inner-shell excitation yields a cross section of 229 Mb (1 Mb $=1.0\times10^{-18}$ cm^2) at a threshold of 38.2 eV. Thus, the total ionization cross section from distorted-wave theory is about a factor of 3 higher than the present measurements at the peak.

The experimental measurements for the ionization cross section of Mo^{2+} are compared with distorted-wave theory in Fig. 4. At 60-eV incident energy, near the peak of the cross section, the measurements are about 10% higher than the configuration-average distorted-wave calculation for $4d$ subshell direct ionization from the $4p^6 4d^4$ ground configuration. For direct ionization of the $4p$ subshell, some of the levels of the $4p^5 4d^4$ configuration will contribute to single ionization, while other levels will contribute to double ionization. A configuration-average calculation for the $4p \rightarrow 4d$ inner-shell excitation yields a cross section of 181 Mb at a threshold of 38.9 eV. Thus, the total ionization cross section from distorted-wave theory is almost a factor of 2 higher than the present measurements at the peak. However, this might be expected since the large effects of correlation and continuum coupling are not included in these configuration-average distorted-wave calculations.

B. Mo^{3+}

The distorted-wave theory is expected to become more accurate as the residual charge on an atomic ion becomes larger. This is due, in part, to the increased strength of the central force of the partially screened nucleus and a concurrent reduction in the effect of electron correlation. The experimental measurements for the ionization cross section of Mo^{3+} are compared with distorted-wave theory in Figs. 5 and 6. Configuration-average distorted-wave calculations are made for direct ionization from the $4p^6 4d^3$ ground configuration including both the $4d$ and $4p$ subshells. Direct ionization of the $4s$ subshell will contribute to the double ionization of Mo^{3+}. Configuration-average calculations were carried out for the $4p \rightarrow 4\ell$ ($\ell=2,3$), $4p \rightarrow 5\ell$ ($\ell=0,1,2,3$), $4p \rightarrow 6\ell$ ($\ell=0,1,2,3$), $4s \rightarrow 4d$, and $4s \rightarrow 5\ell$ ($\ell=0,1$) inner-shell excitation cross sections. The $4p \rightarrow 4d$ excitation cross section is by far the largest. The total ionization cross section from distorted-wave theory including the $4p \rightarrow 4d$ excitation is given by the solid curve in Fig. 5, while the chained curve excludes the $4p \rightarrow 4d$ excitation.

There are 68 *LS* terms and 180 *LSJ* levels in the $4p^5 4d^4$ excited configuration of Mo^{3+}, which straddle the

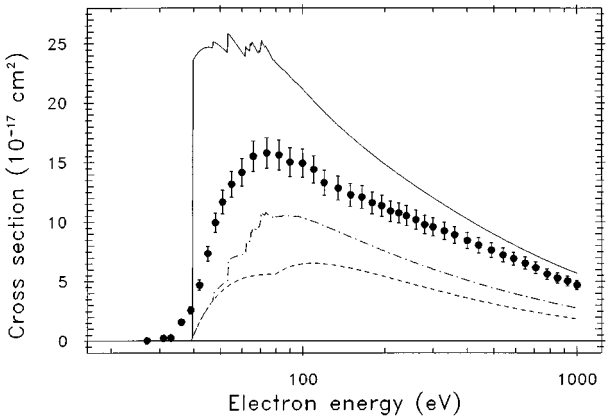

FIG. 5. Electron-impact single ionization of Mo^{3+}. Solid circles: present measurements; solid curve: total ionization from the $4p^6 4d^3$ ground configuration including the $4p \rightarrow 4d$ excitation; dot-dashed curve: total ionization from the $4p^6 4d^3$ ground configuration excluding the $4p \rightarrow 4d$ excitation; dashed curve: direct ionization from the $4p^6 4d^3$ ground configuration.

ionization threshold. Some of the levels of the $4p^5 4d^4$ excited configuration are bound, while other levels may autoionize. Thus, we carried out a level-to-level distorted-wave calculation for the $4p \rightarrow 4d$ excitation to determine the cross section to autoionizing levels only. The total ionization cross section from distorted-wave theory, including only those $4p \rightarrow 4d$ excitations that are able to autoionize, is given by the solid curve in Fig. 6. The good agreement between theory and experiment for Mo^{3+} is somewhat fortuitous, since the partition between bound and autoionizing levels of the $4p^5 4d^4$ configuration will change with only slight shifts in the calculated energies. We used the experimental ionization threshold of 46.4 eV [20] and found that only 44 of the 180 LSJ levels in the $4s^5 4d^4$ excited configuration are able to autoionize and contribute to the ionization cross section.

A better theoretical calculation could be made if the level populations in the $4p^6 4d^3$ ground configuration were known. However, these populations are difficult to determine

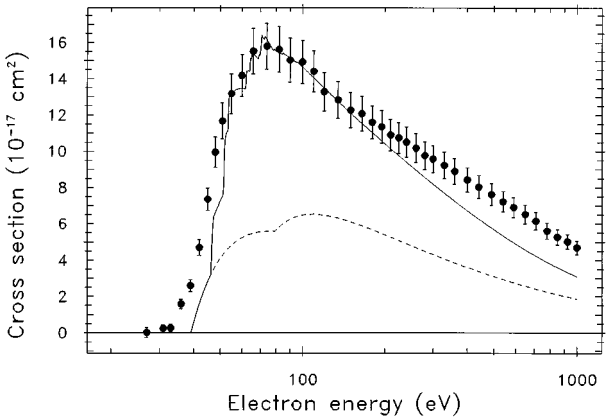

FIG. 6. Electron-impact single ionization of Mo^{3+}. Solid circles: present measurements; solid curve: total ionization from the $4p^6 4d^3$ ground configuration including a level-to-level calculation for the $4p \rightarrow 4d$ excitation; dashed curve: direct ionization from the $4p^6 4d^3$ ground configuration.

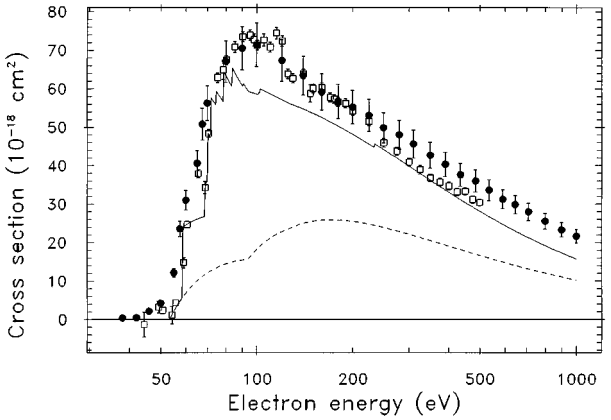

FIG. 7. Electron-impact single ionization of Mo^{4+}. Solid circles: present measurements; solid curve: total ionization from the $4p^6 4d^2$ ground configuration; dashed curve: direct ionization from the $4p^6 4d^2$ ground configuration; open squares: measurements of Bannister *et al.* [6].

experimentally. If the level populations were known, calculations could be carried out to determine a weighted sum of the total ionization cross sections from each ground and metastable level.

C. Mo^{4+} and Mo^{5+}

Two crossed-beam experimental measurements for the ionization cross section of Mo^{4+} are compared with distorted-wave theory in Fig. 7. The present measurements are in good agreement with the previous measurements of Bannister *et al.* [6] over the entire energy range. The present configuration-average distorted-wave calculations are essentially identical to those reported by Bannister *et al.* [6]. Direct ionization calculations from the $4p^6 4d^2$ ground configuration included the $4d$, $4p$, and $4s$ subshells. Inner-shell excitation calculations included the $4p \rightarrow 4f$, $4p \rightarrow 5\ell$ ($\ell = 1,2,3$), $4p \rightarrow 6\ell$ ($\ell = 0,1,2,3$), $4s \rightarrow 4\ell$ ($\ell = 2,3$), $4s \rightarrow 5\ell$ ($\ell = 0,1,2$), and $3d \rightarrow 4\ell$ ($\ell = 2,3$) transitions.

Two crossed-beam experimental measurements for the ionization cross section of Mo^{5+} are compared with distorted-wave theory in Fig. 8. The present measurements are again in good agreement with the previous measurements of Bannister *et al.* [6] over the entire energy range. The present configuration-average distorted-wave calculations are again essentially identical to those reported by Bannister *et al.* [6]. Direct and indirect ionization cross sections are from the $4p^6 4d$ ground configuration and involve the same subshells and transitions as reported above for Mo^{4+}, except the $4p \rightarrow 5p$, which is now bound.

D. Mo^{6+}, Mo^{7+}, and Mo^{8+}

In previous work on the Fe [21] and Ni [22] isonuclear sequences, comparison between distorted-wave theory and ECR crossed-beam experiments indicated that electron-impact ionization from charge states whose ground configurations were $3s^2 3p^n$ occurred mainly from the metastable configurations $3s^2 3p^{n-1} 3d$. We expect the same phenomena to occur in the Mo ions whose ground configurations are $4s^2 4p^n$.

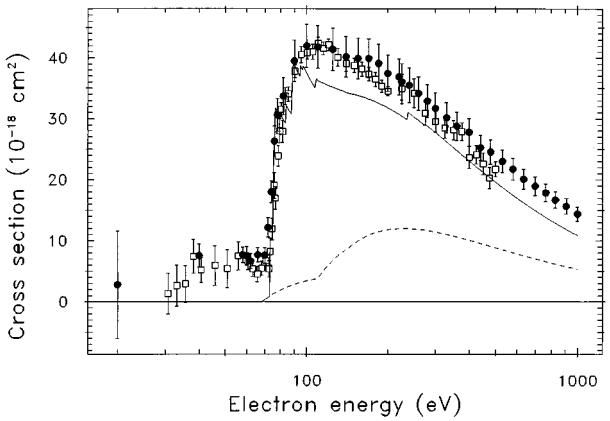

FIG. 8. Electron-impact single ionization of Mo^{5+}. Solid circles: present measurements; solid curve: total ionization from the $4p^6 4d$ ground configuration; dashed curve: direct ionization from the $4p^6 4d$ ground configuration; open squares: measurements of Bannister *et al.* [6].

The experimental measurements for the ionization cross section of Mo^{6+} are compared with distorted-wave theory in Fig. 9. Configuration-average distorted-wave calculations are made for direct ionization from the $4s^2 4p^6$ ground configuration including both the $4p$ and $4s$ subshells and from the $4s^2 4p^5 4d$ metastable configuration including the $4d$, $4p$, and $4s$ subshells. The $4s^2 4p^6$ ground configuration calculations include the $3d \rightarrow 4\ell$ ($\ell = 2,3$) excitations, while the $4s^2 4p^5 4d$ metastable configuration calculations include the $4p \rightarrow 5f$, $4p \rightarrow 6\ell$ ($\ell = 0,1,2,3$), $4s \rightarrow 4f$, $4s \rightarrow 5\ell$ ($\ell = 0,1,2$), and $3d \rightarrow 4\ell$ ($\ell = 1,2,3$) excitations. The calculations for the metastable configuration are in good agreement with experiment in regard to both the threshold for ionization and the magnitude of the cross section. We expect the Mo^{6+} ions from the ECR source are mainly in metastable triplet states of the $4s^2 4p^5 4d$ configuration.

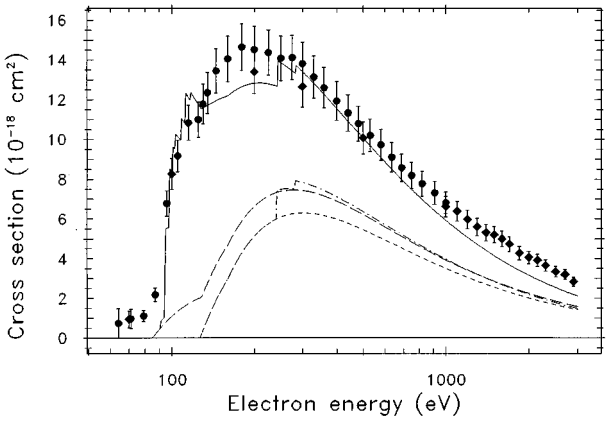

FIG. 9. Electron-impact single ionization of Mo^{6+}. Solid circles: present measurements employing the high-current electron gun; solid diamonds: present measurements employing the high-energy electron gun; solid curve: total ionization from the $4p^5 4d$ metastable configuration; long-dashed curve: direct ionization from the $4p^5 4d$ metastable configuration; dot-dashed curve: total ionization from the $4p^6$ ground configuration; short dashed curve: direct ionization from the $4p^6$ ground configuration.

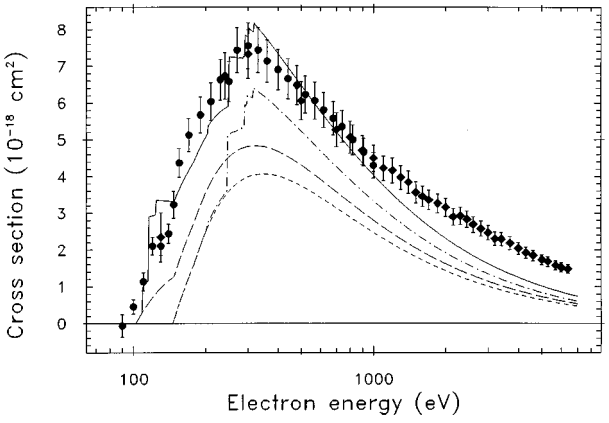

FIG. 10. Electron-impact single ionization of Mo^{7+}. Solid circles: present measurements employing the high-current electron gun; solid diamonds: present measurements employing the high-energy electron gun; solid curve: total ionization from the $4p^4 4d$ metastable configuration; long-dashed curve: direct ionization from the $4p^4 4d$ metastable configuration; dot-dashed curve: total ionization from the $4p^5$ ground configuration; short dashed curve: direct ionization from the $4p^5$ ground configuration.

The experimental measurements for the ionization cross section of Mo^{7+} are compared with distorted-wave theory in Fig. 10. Configuration-average distorted-wave calculations are made for direct ionization from the $4s^2 4p^5$ ground configuration including both the $4p$ and $4s$ subshells and from the $4s^2 4p^4 4d$ metastable configuration including the $4d$, $4p$, and $4s$ subshells. The $4s^2 4p^5$ ground configuration calculations include the $3d \rightarrow 4\ell$ ($\ell = 1,2,3$) and $3d \rightarrow 5\ell$ ($\ell = 0,1,2,3$) excitations, while the $4s^2 4p^4 4d$ metastable configuration calculations include the $4s \rightarrow 4f$, $4s \rightarrow 5\ell$ ($\ell = 1,2$), $3d \rightarrow 4\ell$ ($\ell = 1,2,3$), and $3d \rightarrow 5\ell$ ($\ell = 0,1,2,3$) excitations. The calculations for the metastable configuration are in good agreement with experiment.

The experimental measurements for the ionization cross section of Mo^{8+} are compared with distorted-wave theory in

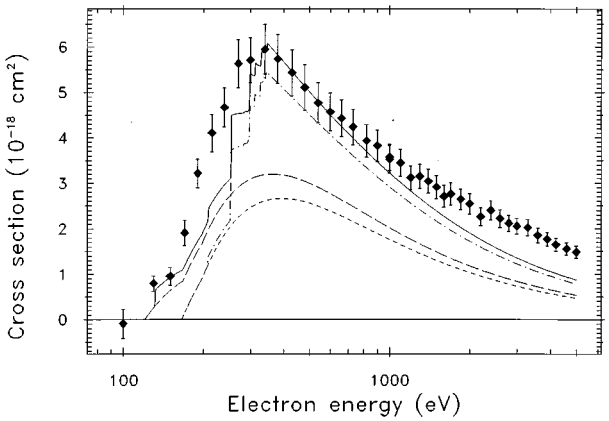

FIG. 11. Electron-impact single ionization of Mo^{8+}. Solid diamonds: present measurements; solid curve: total ionization from the $4p^3 4d$ metastable configuration; long-dashed curve: direct ionization from the $4p^3 4d$ metastable configuration; dot-dashed curve: total ionization from the $4p^4$ ground configuration; short-dashed curve: direct ionization from the $4p^4$ ground configuration.

Fig. 11. Configuration-average distorted-wave calculations are made for direct ionization from the $4s^2 4p^4$ ground configuration including both the $4p$ and $4s$ subshells and from the $4s^2 4p^3 4d$ metastable configuration including the $4d$, $4p$, and $4s$ subshells. The $4s^2 4p^4$ ground configuration calculations include the $3d \rightarrow 4\ell$ ($\ell = 1,2,3$), $3d \rightarrow 5\ell$ ($\ell = 0,1,2,3$), and $3d \rightarrow 6\ell$ ($\ell = 0,1,2,3$) excitations, while the $4s^2 4p^3 4d$ metastable configuration calculations include the $4s \rightarrow 5d$, $3d \rightarrow 4\ell$ ($\ell = 1,2,3$), $3d \rightarrow 5\ell$ ($\ell = 0,1,2,3$), and $3d \rightarrow 6\ell$ ($\ell = 0,1,2,3$) excitations. The calculations for the metastable configuration are again in good agreement with experiment.

V. SUMMARY

The total cross sections for single ionization of molybdenum ions by electron-impact have been investigated for low charge states Mo^+ up to Mo^{8+}. Comparisons with accessible measurements from other groups are in good agreement in nearly the whole observed energy range with the present data within error bars.

The comparison between the distorted-wave theory and the measurements shows that the direct ionization contributions of the calculations underestimate the cross-sections for ions in charge states greater than 2 in the energy range investigated. We find that excitation-autoionization plays an important role, especially at energies between the threshold and the cross-section maximum. A nonvanishing fraction of metastable ions produced in the ECR ion source plasma was found in the primary ion beams. These could not be neglected for charge states greater than 5, where they strongly dominate the primary ion beams. However, as in the case of ions initially in their ground states, the cross sections defined by long-lived metastable ions also show that inner-shell excitation to autoionization levels plays an important role. Generally one can say that the configuration-average distorted-wave calculations with unit branching ratios are in fairly good agreement with respect to both the position and value of the maximum of the observed cross section for ions in charge states greater than 3. However, there are noticeable discrepancies between theory and experiment at both low and high energies. As mentioned before, a better theoretical calculation could be made if the level populations in the target ion were known. These populations are difficult to determine experimentally. If the level populations were known, LSJ level-to-level distorted-wave cacluations with nonunit branching ratios could be carried out to compare with experiment in greater detail.

ACKNOWLEDGMENTS

This work was supported in part by the Deutsche Forschungsgemeinschaft (DFG), Bonn-Bad Godesberg, the Office of Fusion Energy of the U.S. Department of Energy under Contract No. DE-FG05-86-ER53217 with Auburn University and under Contract No. DE-FG05-93-ER54218 with Rollins College, and by a NATO travel grant CRG-940134 with the University of Strathclyde. Computations were carried out at the National Energy Research Supercomputer Center in Livermore, California.

[1] *Atomic and Molecular Processes in Fusion Edge Plasmas*, edited by R. K. Janev (Plenum, New York, 1995).
[2] K. F. Man, A. C. H. Smith, and M. F. A. Harrison, J. Phys. B **20**, 1351 (1987).
[3] J. Oreg, W. Goldstein, P. Mandelbaum, D. Mitnik, E. Meroz, J. L. Schwob, and A. Bar Shalom, Phys. Rev. A **44**, 1741 (1991).
[4] D. Mitnik, P. Mandelbaum, J. L. Schwob, A. Bar Shalom, J. Oreg, and W. H. Goldstein, Phys. Rev. A **50**, 4911 (1994).
[5] K. J. Reed, M. H. Chen, and D. L. Moores, Phys. Rev. A **44**, 4336 (1991).
[6] M. E. Bannister, F. W. Meyer, Y. S. Chung, N. Djuric, G. H. Dunn, M. S. Pindzola, and D. C. Griffin, Phys. Rev. A **52**, 413 (1995).
[7] K. Tinschert, A. Müller, G. Hofmann, K. Huber, R. Becker, D. C. Gregory, and E. Salzborn, J. Phys. B **22**, 531 (1989).
[8] G. Hofmann, A. Müller, K. Tinschert, and E. Salzborn, Z. Phys. D **16**, 113 (1990).
[9] M. Liehr, M. Schlapp, R. Trassl, G. Hofmann, M. Stenke, R. Völpel, and E. Salzborn, Nucl. Instrum. Methods Phys. Res. B **79**, 697 (1993).
[10] R. Becker, A. Müller, A. Achenbach, K. Tinschert, and E. Salzborn, Nucl. Instrum. Methods Phys. Res. B **9**, 385 (1985).
[11] M. Stenke, K. Aichele, D. Hathiramani, G. Hofmann, M. Steidl, R. Völpel, and E. Salzborn, Nucl. Instrum. Methods Phys. Res. B **98**, 573 (1995).
[12] A. Müller, K. Tinschert, C. Achenbach, and E. Salzborn, Nucl. Instrum. Methods Phys. Res. B **10/11**, 204 (1985).
[13] M. S. Pindzola, D. C. Griffin, and C. Bottcher, in *Atomic Processes in Electron-Ion and Ion-Ion Collisions*, Vol. 145 of *NATO Advanced Studies Institute Series B: Physics*, edited by F. Brouillard (Plenum, New York, 1986), p. 75.
[14] R. D. Cowan, *The Theory of Atomic Structure and Spectra* (Univ. of California Press, Berkeley, 1981).
[15] R. D. Cowan and D. C. Griffin, J. Opt. Soc. Am. **66**, 1010 (1976).
[16] S. M. Younger, Phys. Rev. A **22**, 111 (1980).
[17] C. F. Fischer, Comput. Phys. Commun. **64**, 369 (1991).
[18] N. S. Scott and A. Hibbert, Comput. Phys. Commun. **28**, 189 (1982).
[19] H. E. Saraph, Comput. Phys. Commun. **3**, 256 (1972).
[20] C. E. Moore, *Atomic Energy Levels*, Natl. Bur. Stand. (U.S.) Circular No. 35 (U.S. GPO, Washington, DC, 1971), Vol. 3.
[21] M. S. Pindzola, D. C. Griffin, and C. Bottcher, Phys. Rev. A **34**, 3668 (1986).
[22] D. C. Griffin and M. S. Pindzola, J. Phys. B **21**, 3253 (1988).